Article

Magneto-Optical Faraday Effect in Quasicrystalline and Aperiodic Microresonator Structures

Daria O. Ignatyeva [1,2,3,]*[iD], Polina V. Golovko [1,2][iD] and Vladimir I. Belotelov [1,2,3][iD]

1   Russian Quantum Center, 121353 Moscow, Russia
2   Photonics and Quantum Technologies School, Faculty of Physics, Lomonosov Moscow State University, 119991 Moscow, Russia
3   Physics and Technology Institute, Vernadsky Crimean Federal University, 295007 Simfeporol, Russia
*   Correspondence: ignatyeva@physics.msu.ru

Abstract: We theoretically and numerically investigate magnetophotonic microresonators formed by a magnetic layer sandwiched between two reflective multilayers with different layer arrangements. Quasicrystals with the Fibonacci layer sequence and aperiodic structures with the Thue–Morse sequence are all compared to the conventional photonic crystal Bragg microresonators. The magneto-optical spectral properties of such magnetophotonic structures are completely different from each other and from a uniform magnetic film. In multilayered structures of various order types, microresonator modes are excited. The feature of multilayered structures with arrangements different from a periodic one is that they support the excitation of the multiple microresonator modes in a limited visible and near-infrared spectral range. The wavelengths of the two microresonator modes in a regular photonic crystal differ by more than one octave. This feature of the quasi-crystalline and aperiodic microresonators is important for applications in devices based on the Faraday effect.

1. Introduction

The magneto-optical Faraday effect [1] is one of the most important magneto-optical effects being used in various applications [2], such as isolators [3], modulators [4], routers and deflectors [5], sensors [6,7], and magnetometers [8,9]. The magneto-optical Faraday rotation Φ for thick films and crystals is proportional to the crystal thickness d and a specific Faraday rotation angle ϕ, so $\Phi = \phi d$, where ϕ is determined by the material parameters. That is why the trend towards device miniaturization inevitably results in the decrease in the Faraday rotation Φ. Thus, new methods of increasing the Faraday rotation, for example, by means of nanophotonics, are required [10,11].

Magnetophotonic crystals are known as one of the most efficient structures that enhance the Faraday rotation [12,13]. Magnetophotonic crystals are periodic structures containing magnetic materials with the refractive index changing in one, two or three dimensions with a period comparable to the light wavelength [14]. Photonic crystals are characterized by a photonic bandgap in terms of the energy of photons. Light with frequencies that lie in the photonic bandgap cannot propagate through the photonic crystal, giving rise to the phenomenon of Bragg reflection. Multiple re-reflections of light inside a periodic magnetophotonic crystal at the bandgap edges enhance the effective length of the magnetic material that is passed by the light during these re-reflections. As a consequence, this increases the efficiency of the magneto-optical interaction and enhances the Faraday rotation angles [15–17]. Even higher Faraday rotation enhancement can be observed if a magnetic defect is sandwiched between the two photonic crystals, so that the whole structure acts as a Fabry–Perot microresonator with the Bragg mirrors surrounding it [18–22]. Such an increase in the magneto-optical response can be explained by the

implementation of a multi-pass mode inside the magnetic microresonator layer [13]. Similar phenomena are observed under the excitation of the photonic crystal surface states (optical Tamm states [23]) excited about the interface between the two different photonic crystals or at the surface of a single photonic crystal [24–26].

The photonic crystals' bandgap structure is regular because of their periodicity. Several advances in modern nanophotonics are associated with the ability to manipulate the structural order to obtain the desired spectral properties. There are several types of ordering: periodic in real and discrete in reciprocal space, aperiodic in real space and discrete in reciprocal space, and aperiodic in both real and reciprocal spaces. From this point of view, photonic crystals are described by the periodic spatial permittivity function in real space as well as by the discrete reciprocal lattice function. This mimics the natural order of the atoms in the crystal lattices. At the same time, there is another type the ordered structure with discrete spectra in the reciprocal space, namely so-called quasicrystals [27]. Quasicrystals are non-periodic in real space, but possess long-range order and have self-similarity properties. Natural materials with quasicrystalline structure are quite rare, however, they exist [28]. The important difference between quasicrystalline and periodic crystalline structures is the absence of translational symmetry and the presence of only long-range scales ordering. Quasicrystals with a dimensionality of nD (n = 1, 2 or 3) can be represented as a partial projection of an appropriate periodic structure in a higher dimensional space mD, where $m > n$ [29]. One-dimensional quasicrystalline structures include, for example, the ones based on a Fibonacci sequence [30]. A Fibonacci binary sequence (so-called Fibonacci word) is a sequence in which the first two elements are $S_1 = 0$ and $S_2 = 01$, and each subsequent number is calculated based on the two previous numbers as $S_n = S_{n-1}S_{n-2}$ [31]. An alternative definition of a binary Fibonacci word leading to exactly the same sequence is based on a substitution rule. The S_n Fibonacci sequence term is obtained by substitution $1 \rightarrow 0$ and $0 \rightarrow 01$ in the S_{n-1} term. This structure is interesting for research because the sequence is symmetric with respect to the permutations of 1 and 0 [32–34]. Two approaches to constructing the Fibonacci series involve either substitution or partial projection from a two-dimensional square lattice [35]. Photonic structures based on Fibonacci quasicrystal layer ordering are reported to have significantly different optical properties from those of the periodic photonic crystals. Photonic quasicrystals also have bandgaps, however, their spectral position is not equidistant as for the regular photonic crystals [29]. Besides the quasicrystals, there are other deterministic aperiodic structures possessing discrete Fourier spectra, long-range order and self-similarity properties, and lacking periodicity in the real space. For example, such structures could be designed based on Thue–Morse [36], Cantor and period-doubling sequences [37,38]. Their optical spectra are also unusual compared to the regular periodic structures and they exhibit an irregular bandgap structure [39–41]. Such aperiodic ordered structures attract significant interest in all-dielectric nanophotonics [42] and plasmonics [43].

Recent research has focused on the magneto-optics of quasicrystalline and aperiodic deterministic structures. It was revealed that the Faraday rotation can be enhanced in Fibonacci [44,45] and Octonacci [46] types of quasiperiodic magnetophotonic structures. Non-reciprocity in transmittance [47–49], radiation [50] and absorption [51], as well as the broadband non-reciprocal absorption [52] and tunability of the Goos–Hanhen shift [53] were revealed for nanophotonic aperiodic deterministic structures with in-plane magnetization.

The scope of the present study was the theoretical and numerical investigation of a magnetophotonic microresonator formed by a magnetic layer sandwiched between two multilayers with different layer arrangements: periodic, quasicrystalline, and aperiodic, as can be seen in Figure 1. As was mentioned above, the optical spectral properties of such multilayers are completely different from each other and constitute a uniform magnetic film. In the present study, we revealed the impact of the periodicity type of the multilayer forming the mirrors surrounding the microcavity on the magneto-optical properties of the structure.

We demonstrate that microresonator modes can be excited in multilayered structures of various order types. The most remarkable result of the present study is that multilayered structures with different arrangements from those of a periodic one support the excitation of the multiple microresonator modes in a limited visible and near-infrared spectral range. At the same time, the wavelengths of the two microresonator modes in a regular photonic crystal differ by more than one octave. This feature is important for applications in devices based on the Faraday effect.
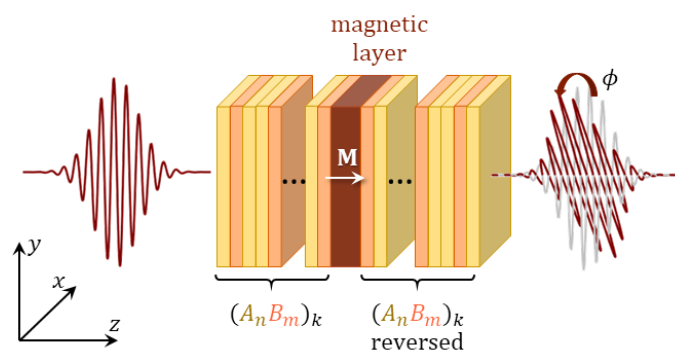

Figure 1. The scheme illustrating the considered configuration of a Faraday rotation in the microresonators formed by multilayered structures with different layer arrangements and a magnetic layer. The multilayers labeled as $(A_n B_m)_k$ are formed by non-magnetic dielectric layers, denoted as *A* and *B*, correspondingly arranged in various sequences of periodic, quasicrystalline and aperiodic ordering (see Materials and Methods for the details and Table 1).

Table 1. Photonic crystal, quasi-crystal and aperiodic Thue–Morse multilayer compositions.

Type	Multilayer Composition
Photonic crystal	A B A B A B A B A B
Quasicrystal	A B A A B A B A A B A A B
Thue–Morse sequence	A B B A B A A B B A A B A B B A B A A B A B B A A B B A B A A B

2. Materials and Methods

The numerical simulations of optical and magneto-optical response were carried out using the original program, performing the numerical solution of Maxwell's equations using the RCWA (rigorous coupled-wave analysis) method [54,55]. The RCWA method provides the optical characteristics of a multilayered structure, such as transmittance, reflectance, absorption, polarization rotation, among others. The magneto-optical properties of the structure are taken into account as the non-diagonal elements of the permittivity tensor, so that $\varepsilon_{ij} = i\epsilon_{ijk}g_k$ [56], where ϵ_{ijk} is a Levi–Civita symbol and g_k are the components of the gyration vector that is parallel to the magnetization of the material.

We considered a magnetic layer surrounded by two identical non-magnetic multilayers symmetrically deposited with respect to the magnetic layer (see the sketch in Figure 1). Multilayers are formed by the non-magnetic dielectric layers denoted by *A* and *B*, which are arranged in various sequences of periodic, quasicrystalline and aperiodic ordering (the details are provided below). The entire structure was supposed to be deposited on a silica glass substrate with $n_{\text{SiO2}} = 1.45$.

The magnetic layer has $d_{\text{mr}} = 160$ nm thickness and $n_{\text{mr}} = 2.5 + 0.05i$, so it is a half-wavelength layer for $\lambda = 800$ nm wavelength. The permittivity and magneto-optical properties of the magnetic layer were taken equal to those of the bismuth-substituted iron-garnet, $(\text{BiY})_3\text{Fe}_5\text{O}_{12}$ which is widely used as a transparent magnetic dielectric in the magneto-optical studies. An external magnetic field is applied along *z* axis that coincides with the light propagation direction, see Figure 1. Magnetic layer magnetization is taken into account as the non-diagonal elements of the permittivity tensor $\varepsilon_{\text{mr}}^{xy} = -\varepsilon_{\text{mr}}^{yx} = ig$ [57]. For magnetic materials, such as iron-garnets, for example, gyration $g_{\text{mr}}(\lambda)$ significantly

depends on a wavelength [58,59]. Moreover, the specific Faraday rotation is equal to $\phi = -\pi g_{mr}/(n_{mr}\lambda)$, so it decreases with an increasing wavelength. As we would like to reveal the spectral peculiarities associated with a structural order and to compare the enhancement at the different wavelengths, all the Faraday rotation spectra were normalized on the $\phi_0(\lambda) = -\pi g_{mr}/(n_{mr}\lambda)$ value, where the dispersion $g_{mr}(\lambda)$ was taken into account. Notice that ϕ_0 itself does not take into account the interference effects that take place in thin [60] and structured [61] films.

Three types of multilayered structures surrounding a magnetic layer were considered, as can be seen in Table 1), where A and B denote the corresponding dielectric layer. We considered these layers to possess $n_A = 2.0$, $d_A = 100$ nm and $n_B = 1.5$, $d_B = 133$ nm refractive indices and thicknesses, respectively, which correspond to the typical materials used for the multilayer fabrication, such as Ta_2O_5 and SiO_2, for example. The multilayers to the right and to the left of the magnetic layer were arranged symmetrically with respect to it. The first type is the regular photonic crystal containing alternating $\lambda/4$ layers (Table 1). The second one is a quasicrystal with the same layers arranged according to the Fibonacci sequence. The n-th element of the Fibonacci sequence S_n is formed using a recursive formula: $S_1 = A$, $S_2 = AB$, $S_n = S_{n-1}S_{n-2}$. We choose the sixth term of this sequence for a detailed analysis (Table 1). The third type is an aperiodic Thue–Morse structure, which is also formed using the same layers by the following recursive formula: $S_1 = A$, $S_n = S_{n-1}\bar{S}_{n-1}$, where $\bar{S}_{n-1}$ is a sequence S_{n-1} with a replacement $A \leftrightarrow B$. Notice that, as the Fibonacci and Thue–Morse sequences contain repeating elements, some of the layers in the structure have double thickness and the total number of the layers is therefore smaller than the number of the sequence terms in Table 1. Simultaneously, the thicknesses of layers forming Fibonacci and Thue–Morse structures are multiples of d_A and d_B. Actually, the number of layers in the considered Fibonacci structure is 10, which is equals to the number of layers in a regular periodic photonic crystal (as can be seen in Table 1). The number of layers in the considered Thue–Morse structure is 22. As it will be shown below, the microresonator-type features of such Thue–Morse multilayer structures require a larger number of elements than in the case of periodic and quasiperiodic structures. The isolated bare magnetic layer on a glass substrate was also considered a reference.

3. Results and Discussion

While the difference between the regular photonic crystal, quasicrystal, and aperiodic structures in real space is obvious, it is important that they also differ in the reciprocal space. Figure 2 shows the Fourier spectra $\tilde{\varepsilon}(K) = |\frac{1}{\sqrt{2\pi}} \int_0^L \tilde{\varepsilon}(z) \exp(iKz) dz|$ of the corresponding multilayer (see Table 1) permittivity spatial distribution $\tilde{\varepsilon}(z) = \varepsilon(z) - \langle \varepsilon(z) \rangle$, where L is the total length of the multilayer. The mean value of the permittivity $\langle \varepsilon(z) \rangle = \frac{1}{L} \int_0^L \varepsilon(z) dz$ was subtracted to obtain a clearer picture, and the values of K were normalized on $G_0 = 2\pi/(d_A + d_B)$.
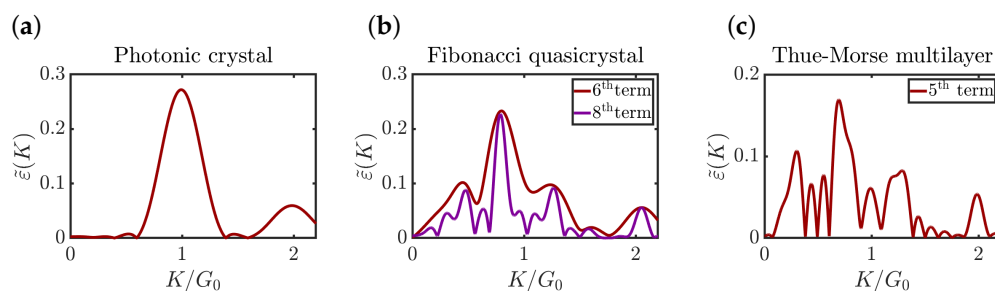

Figure 2. Fourier spectra $\tilde{\varepsilon}(K)$ of the multilayer permittivity spatial distribution $\tilde{\varepsilon}(z) = \varepsilon(z) - \langle \varepsilon(z) \rangle$ for (**a**) photonic crystal; (**b**) Fibonacci quasicrystal; (**c**) Thue–Morse multilayer (see Table 1).

The $\tilde{\varepsilon}(K)$ spectra of a photonic crystal show a regular periodic collection of peaks corresponding to $G_m = mG_0$, $m \in \mathbb{N}$. The Fibonacci quasicrystal $\tilde{\varepsilon}(K)$ spectrum likewise features peaks, but their arrangement is non-periodic. The position of these peaks can

be numerically estimated as $G_{m_1,m_2} = \frac{(m_1 + m_2/t)}{2} G_0$, where $m_{1,2} \in \mathbb{N}$, and $t = N_A/N_B$ is the ratio of numbers of A-type and B-type elements [62,63]. For the sixth term of the Fibonacci sequence (see Table 1) $t = 1.6$ which is quite close to a limit for an infinite Fibonacci sequence $t \to \sqrt{5} + 1/2$. Actually, this fact causes the Fibonacci $\tilde{\varepsilon}(K)$ spectra to be the same for different numbers of layers (see Figure 2b). The spectra $\tilde{\varepsilon}(K)$ of the infinite Thue–Morse structure has peaks at $G_m = mG_0/2$, $m \in \mathbb{N}$, similar to the regular photonic crystal [62,63]. However, for a finite number of layers, the spectra $\tilde{\varepsilon}(K)$ has even more pronounced additional peaks in the considered region than the periodic ones (see Figure 2c). This will result in more complicated transmittance and Faraday rotation spectra.
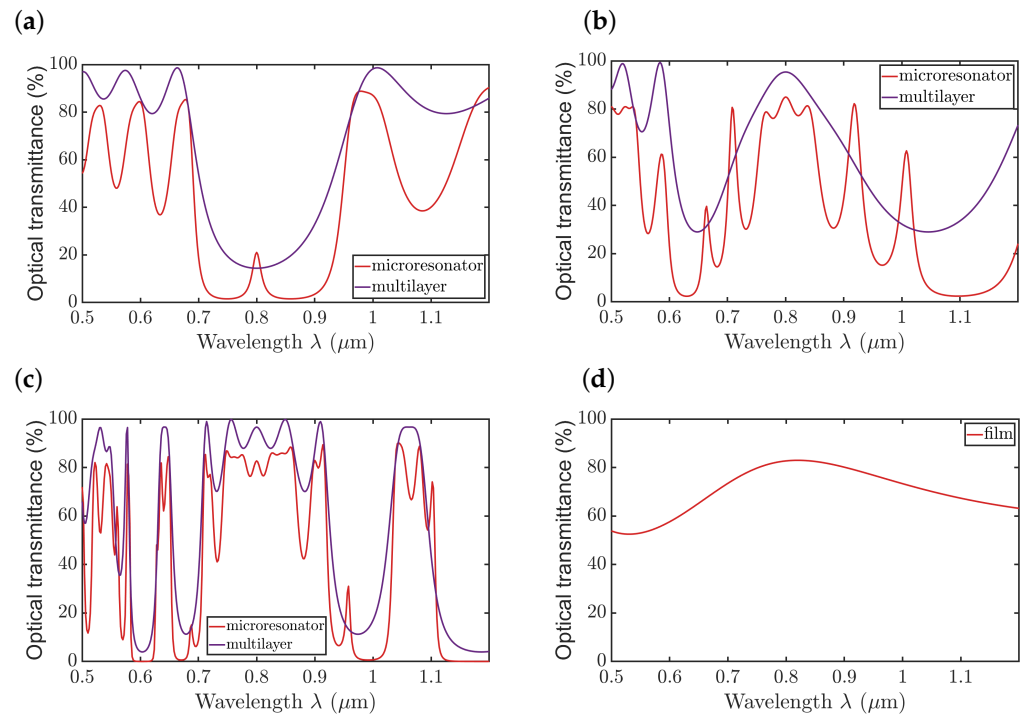

Figure 3. Optical transmittance vs. wavelength λ (angle of incidence $\theta = 0$ deg) spectra for multilayers and corresponding microresonators formed based on (**a**) photonic crystal; (**b**) Fibonacci quasicrystal; (**c**) Thue–Morse structure; (**d**) optical transmittance of a bare magnetic film. Violet lines labeled as 'multilayer' and red lines labeled as 'microresonator' denote the transmittance of the corresponding multilayers and microresonators formed by a magnetic layer sandwiched between them.

The optical transmittance spectra for the four types of structures are quite different, as can be seen in Figure 3. The photonic crystal microresonator structure (Figure 3a) exhibits a rather wide bandgap at 0.7 μm $\leq \lambda \leq 0.9$ μm wavelengths observed as a transmittance zero. Outside the bandgap, a regular set of transmittance maxima and minima are observed, corresponding to the interference in the whole multilayered slab. A microresonator mode is clearly seen at $\lambda = 0.8$ μm as a narrow transmittance peak at the center of a bandgap. According to the photonic crystal theory, the second, third, …, m-th bandgaps have centers at: $\lambda_{bg}^m = 2(n_A d_A + n_B d_B)/(2m - 1)$ wavelength. The existence of the microresonator mode in a regular photonic crystal is determined by $\lambda_{mr} = 2n_{mr} d_{mr}/(2m - 1)$, $m \in \mathbb{N}$. As we consider the limited part of the visible and near-infrared range, only one bandgap and one were microresonator mode observed in this range.

The excitation of the microresonator mode results in a light energy concentration inside the magnetic layer. This is the physical origin of the enhancement of the Faraday rotation that will be discussed below. To prove the energy concentration at the wavelengths that are identified as the microresonator mode resonances, we performed simulations of the distribution of the light intensity E^2 inside the magnetophotonic microresonators, as can be

seen in Figure 4. Field enhancement in the magnetic layer is observed for the mentioned wavelengths in all the multilayered ordering types.

In contrast to the photonic crystal, the quasi-crystal microresonator structure (Figure 3b) has two shallow bandgaps at the neighboring frequency regions, 0.6 μm $\leq \lambda \leq$ 0.7 μm and 0.9 μm $\leq \lambda \leq$ 1.2 μm. Their positions correspond to the positions of the peaks in the quasicrystal $\tilde{\varepsilon}(K)$ spectra (Figure 2). In each of the bandgaps, the microresonator mode is observed, at λ = 0.662 μm and λ = 1.010 μm (see also Figure 4c,d). This is an unusual phenomenon compared to the case of the periodic structures. Notice that the transmittance of the microresonator-mode resonance is twice as high as in the case of the photonic crystal. This is due to a fact that the quasicrystal at its bandgap provides less efficient reflection than a regular photonic crystal with quarter-wavelength layers.
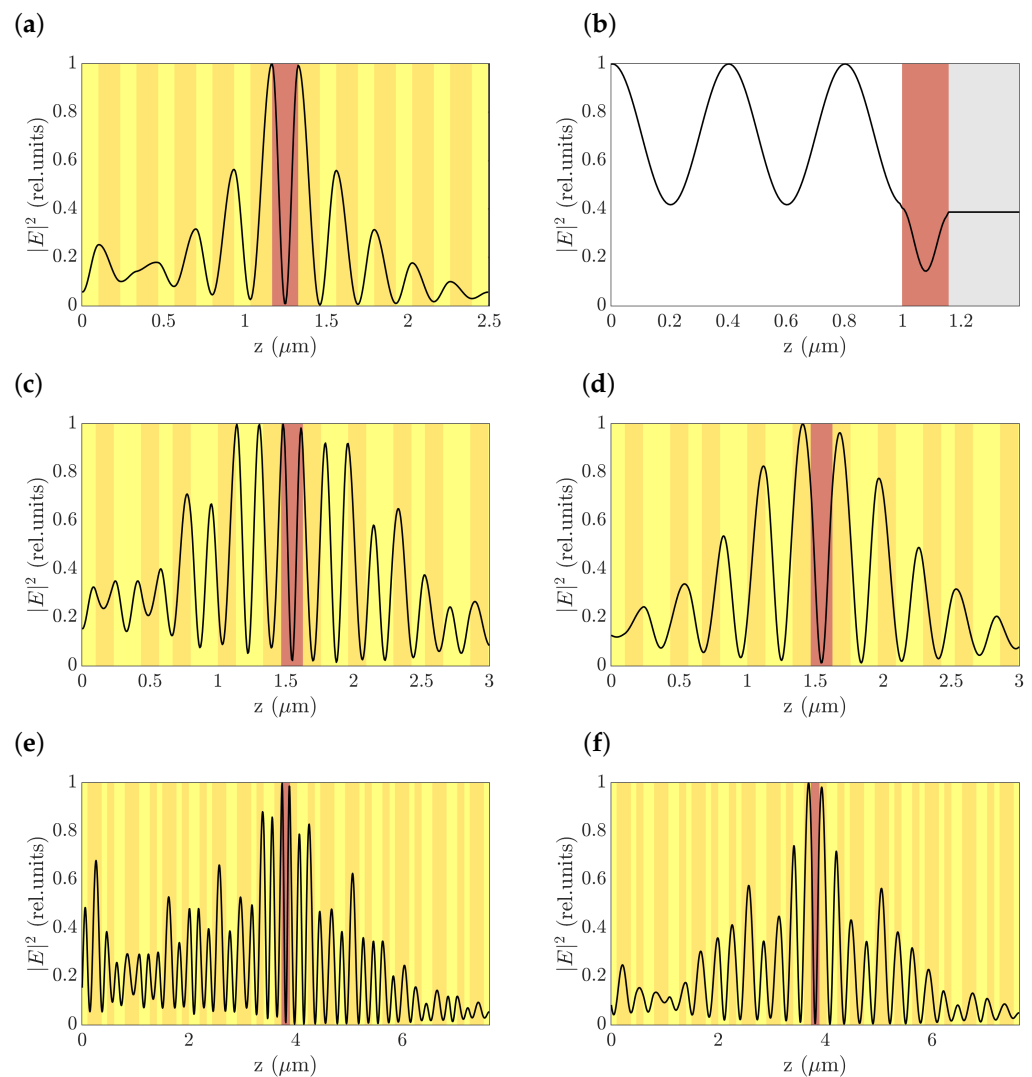

Figure 4. The distribution of the electromagnetic field magnitude $|E|^2$ for microresonator modes excited in multilayers based on (**a**) photonic crystal at the wavelength 800 nm; (**b**) just a bare magnetic film at 800 nm; (**c**,**d**) Fibonacci quasicrystal at the wavelengths; (**c**) 662 nm and (**d**) 1010 nm; (**e**,**f**) Thue–Morse multilayer at the wavelengths (**e**) 686 nm and (**f**) 958 nm.

The Thue–Morse microresonator structure (Figure 3c) has several bandgaps where the transmittance decreases. The interference pattern outside the bandgap is represented by an aperiodic set of transmittance maxima and minima due to the irregularity of the quasicrystal in real space. One may notice that the transmittance spectra of the Thue–Morse structure is much richer with transmittance dips and peaks compared to the regular photonic crystal and quasicrystal, but its analytical description is also more complicated. The bandgaps are

located at 0.58 μm $\leq \lambda \leq$ 0.62 μm, at 0.66 μm $\leq \lambda \leq$ 0.72 μm, at 0.9 μm $\leq \lambda \leq$ 1.1 μm, and at $\lambda >$ 1.1 μm. Two of these bandgaps that are the nearest to $\lambda \sim$ 0.8 μm $= 4d_{mr}n_{mr}$ contain the resonances corresponding to the microresonator modes (as can also be seen in Figure 4e,f).

For the sake of comparison, we also show the transmittance spectra of a bare film, as can be seen in Figure 3d. One may see the interference maxima (see also Figure 4b) at $\lambda =$ 0.8 μm which is broad due to the small thickness of the film. Actually, the difference between the transmittance maxima and minima is not significant for the film, and it also causes a change in the Faraday rotation, as will be demonstrated subsequently.

Figure 5 shows that the specific Faraday rotation spectra have distinct maxima near the spectral positions of the transmittance peaks (see Figure 3 for a comparison). At the same time, the magnitude of these peaks is significantly different for the different structure types. For a bare film (Figure 5d), the specific Faraday rotation changes due to an interference of less than 25% from its value ϕ_0 in a uniform film where the interference is suppressed. High enhancement reaching 8 times is obtained for a traditional photonic crystal microresonator (Figure 5a) under the excitation of the microresonator mode. This agrees well with the experimental and numerical results presented in the other studies for similar structures (see [18–21]).

A quasicrystal is a less efficient reflector than a regular periodic photonic crystal, so that the Faraday rotation observed at the microresonator mode excitation wavelengths is twice as small as in the photonic crystal. The enhancement of the specific Faraday rotation reaches four times. It is possible to compensate for the smaller reflectivity of the quasicrystal by using a multilayer with a larger number of layers. According to the Fibonacci crystal analysis, the position of the spectral features would not change in this case (as can be seen in Figure 2b). Simultaneously, increasing the number of layers increases the efficiency, resulting in an increase in the Faraday rotation (as can be seen in Figure 5b). Therefore, similarly to the photonic crystal microresonator structures, it is possible to vary the number of layers forming it to achieve higher efficiency and enhancement.
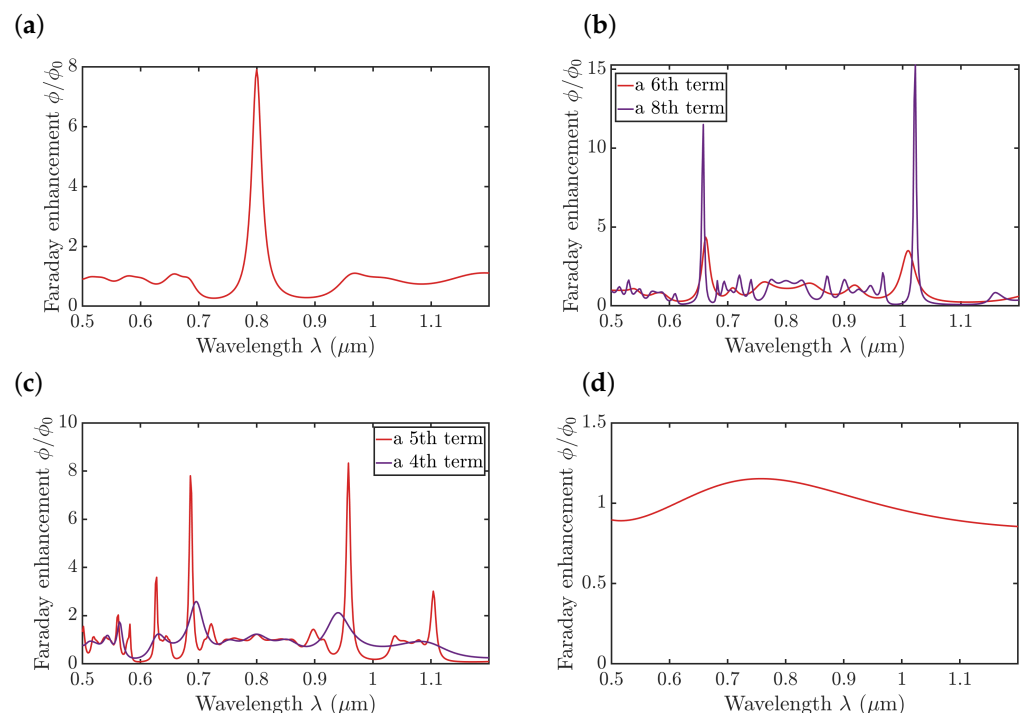
(a)

(b)

(c)

(d)

Figure 5. The Faraday rotation spectra normalized to a uniform film value ϕ/ϕ_0 for microresonators based on the (**a**) photonic crystal; (**b**) quasicrystal crystal; (**c**) Thue–Morse structure; and (**d**) bare magnetic film. Notice the *y* axis scale difference.

The enhancement of the Faraday rotation at the microresonator mode positions is clearly seen for the Thue–Morse-sequence-based structure (Figure 5c). Such a structure can also localize light in a magnetic microresonator layer (see Figure 4e,f). At the same time, the number of layers required for such enhancement is higher than in the case of a regular photonic crystal. As shown in Figure 5c), the Thue–Morse structure with 11 layers (fourth term of the sequence) provides a very moderate enhancement compared to the smooth film. At the same time, the Faraday effect enhancement observed for 22 layers (fifth term of the sequence) is high.

Figure 6 shows that the resulting magneto-optical enhancement at the peaks corresponding to microresonator modes in the microresonators formed between the regular photonic crystals and aperiodic deterministic multilayers can be the same if the number of layers N in the multilayered structure is properly adjusted. Figure 6a shows how the relative Faraday enhancement at the peaks corresponding to microresonator modes change with the increase in the number of layers N in the multilayered structure.The enhancement in a regular photonic crystal is clearly saturated for $N \sim 16$. Such a behavior is observed when the effective propagation length inside a magnetic defect reaches the decay length determined by its absorption. This makes the Fibonacci quasicrystal with numerous layers provide similar Faraday enhancement as the periodic photonic crystal. At the same time, an important point is that both Fibonacci and Thue–Morse multilayers support multiple microresonator resonances.
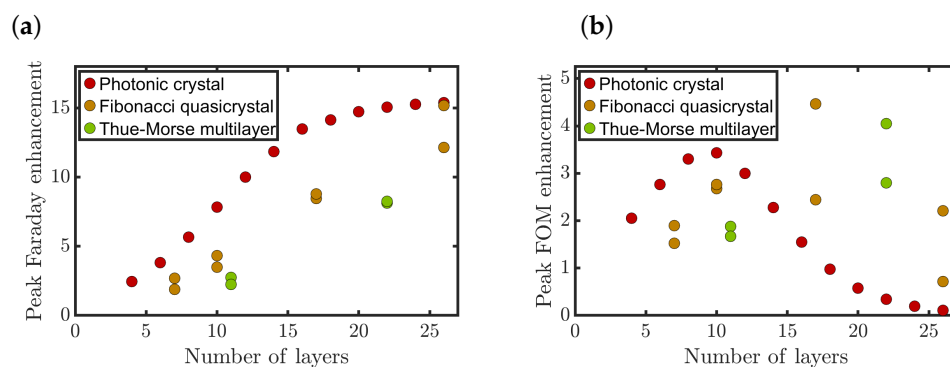
(a)   **(b)**

Figure 6. (**a**) The relative Faraday effect and (**b**) peak FOM enhancements at the peaks corresponding to microresonator modes in photonic crystal, quasicrystal and Thue–Morse structures (see the legend) as a function of the number of layers in the structure.

From a practical point of view, the balance between the enhancement of the magneto-optical effects and all types of losses due to absorption and back-reflection is important. While the Faraday rotation is expected to increase linearly with the increase in the effective path in a magnetic material, the dependence of absorption in this layer and the reflectance of the multilayers on the layer numbers is nonlinear. The level of the magneto-optical signal measured by the detector is determined by the Faraday rotation Φ and the detector noise defined by the fluctuations of the laser intensity transmitted through the structure and characterized by $\Delta T / \sqrt{T}$ magnitude [9]. Thus, the value of the magneto-optical figure of merit determined as MOFOM $= |\phi| \sqrt{T}$ was analyzed for all types of the structures (Figure 6b). It is clearly seen that while the layer number increases, the MOFOM reaches its maxima value for the multilayered structure with a certain number of layers and then decreases. Thus, for real structures, there is always a trade-off between magneto-optical enhancement and signal level reduction. At the same time, MOFOM enhancement also reaches similar values of 3.5–4 times for the regular photonic crystals and aperiodic deterministic structures with an appropriate number of layers (Figure 6b).

The appearance of multiple microresonator modes is a most important and general property of the multilayered non-periodic structures possessing neighboring bandgaps, whose positions are determined by the multilayer parameters. An ability to control the positions of these bandgaps and the consequent positions of the microresonator modes

excited in magnetic materials by multilayer design might be an interesting direction for future research.

Summing up, we demonstrated that quasicrystal and aperiodic multilayered structures based on Fibonacci and Thue–Morse sequences support the excitation of the two microresonator modes in a limited range of visible and near-IR wavelengths. Their wavelengths are determined by the Bragg reflection conditions formed in a multilayered structure. The efficiency of the Bragg mirrors based on aperiodic and quasicrystal structures is smaller, so a higher number of layers is required to achieve significant enhancement (Figure 6). At the same time, an interesting feature of such structures is their ability to excite several modes and tune their position through structure design.

4. Conclusions

In the present study, magnetophotonic cavities formed by a magnetic layer sandwiched between two reflective multilayers with different layer arrangements were investigated. Ordinary periodic photonic crystals, quasicrystals with the Fibonacci layer sequence, and aperiodic structures with the Thue–Morse sequence of layer arrangements are considered. The magneto-optical spectral properties of such magnetophotonic structures are completely different from each other and from a uniform magnetic film. In multilayered structures of various order types, microresonator modes localized in the magnetic layer and providing enhanced Faraday rotation are excited. The feature of multilayered structures with arrangements different from a periodic one is that they support the excitation of the multiple microresonator modes in a limited visible and near-infrared spectral range. At the same time, the wavelengths of the multiple microresonator modes in a regular photonic crystal differ by more than one octave. This feature of the quasi-crystalline and aperiodic multilayered structures significantly enriches the resonant magneto-optical spectra of the magnetophotonic structures and is therefore important for applications in devices based on the Faraday effect.

References

1. Faraday, M. On the magnetization of light and the illumination of magnetic lines of force. *Philos. Trans. R. Soc. Lond.* **1846**, *136*, 1–20.
2. Kimel, A.; Zvezdin, A.; Sharma, S.; Shallcross, S.; De Sousa, N.; García-Martín, A.; Salvan, G.; Hamrle, J.; Stejskal, O.; McCord, J.; et al. The 2022 magneto-optics roadmap. *J. Phys. Appl. Phys.* **2022**, *55*, 463003. [CrossRef]
3. Karki, D.; El-Ganainy, R.; Levy, M. Toward high-performing topological edge-state optical isolators. *Phys. Rev. Appl.* **2019**, *11*, 034045. [CrossRef]
4. Silva, C.; Guedes, M.; Pereira, N.; Alvarenga, A. Assembly of a Faraday modulator for polarimetric measurements. In Proceedings of the Journal of Physics: Conference Series, Brasilia, Brazil, 23–27 June 2015; IOP Publishing: Bristol, UK, 2015; Volume 575, p. 012019.

5.　Ho, K.S.; Im, S.J.; Pae, J.S.; Ri, C.S.; Han, Y.H.; Herrmann, J. Switchable plasmonic routers controlled by external magnetic fields by using magneto-plasmonic waveguides. *Sci. Rep.* **2018**, *8*, 1–8. [CrossRef]

6.　Maccaferri, N.; E Gregorczyk, K.; De Oliveira, T.V.; Kataja, M.; Van Dijken, S.; Pirzadeh, Z.; Dmitriev, A.; Åkerman, J.; Knez, M.; Vavassori, P. Ultrasensitive and label-free molecular-level detection enabled by light phase control in magnetoplasmonic nanoantennas. *Nat. Commun.* **2015**, *6*, 1–9.

7.　Rizal, C.; Manera, M.G.; Ignatyeva, D.O.; Mejía-Salazar, J.R.; Rella, R.; Belotelov, V.I.; Pineider, F.; Maccaferri, N. Magnetophotonics for sensing and magnetometry toward industrial applications. *J. Appl. Phys.* **2021**, *130*, 230901. [CrossRef]

8.　Fujikawa, R.; Tanizaki, K.; Baryshev, A.; Lim, P.B.; Shin, K.H.; Uchida, H.; Inoue, M. Magnetic field sensors using magnetophotonic crystals. In Proceedings of the Photonic Crystals and Photonic Crystal Fibers for Sensing Applications II, SPIE, 2006, Boston, MA, USA, 1–4 October 2006; Volume 6369, pp. 85–92.

9.　Ignatyeva, D.O.; Knyazev, G.A.; Kalish, A.N.; Chernov, A.I.; Belotelov, V.I. Vector magneto-optical magnetometer based on resonant all-dielectric gratings with highly anisotropic iron garnet films. *J. Phys. Appl. Phys.* **2021**, *54*, 295001. [CrossRef]

10.　Lodewijks, K.; Maccaferri, N.; Pakizeh, T.; Dumas, R.K.; Zubritskaya, I.; Åkerman, J.; Vavassori, P.; Dmitriev, A. Magnetoplasmonic design rules for active magneto-optics. *Nano Lett.* **2014**, *14*, 7207–7214. [CrossRef]

11.　Belotelov, V.; Zvezdin, A. Magnetooptics and extraordinary transmission of the perforated metallic films magnetized in polar geometry. *J. Magn. Magn. Mater.* **2006**, *300*, e260–e263. [CrossRef]

12.　Lyubchanskii, I.; Dadoenkova, N.; Lyubchanskii, M.; Shapovalov, E.; Rasing, T. Magnetic photonic crystals. *J. Phys. Appl. Phys.* **2003**, *36*, R277. [CrossRef]

13.　Inoue, M.; Baryshev, A.; Goto, T.; Baek, S.; Mito, S.; Takagi, H.; Lim, P. Magnetophotonic crystals: Experimental realization and applications. *Magnetophotonics* **2013**, *178*, 163–190.

14.　Sakoda, K. *Optical Properties of Photonic Crystals*; Springer Science & Business Media: Berlin/Heidelberg, Germany, 2004; Volume 80.

15.　Inoue, M.; Yamamoto, T.; Isamoto, K.; Fujii, T. Effect of structural irregularity on propagation properties of optical waves in discontinuous magneto-optical media with one-dimensional quasirandom aray structures. *J. Appl. Phys.* **1996**, *79*, 5988–5990. [CrossRef]

16.　Steel, M.; Levy, M.; Osgood, R. High transmission enhanced Faraday rotation in one-dimensional photonic crystals with defects. *IEEE Photonics Technol. Lett.* **2000**, *12*, 1171–1173. [CrossRef]

17.　Koerdt, C.; Rikken, G.; Petrov, E. Faraday effect of photonic crystals. *Appl. Phys. Lett.* **2003**, *82*, 1538–1540. [CrossRef]

18.　Inoue, M.; Arai, K.; Fujii, T.; Abe, M. Magneto-optical properties of one-dimensional photonic crystals composed of magnetic and dielectric layers. *J. Appl. Phys.* **1998**, *83*, 6768–6770. [CrossRef]

19.　Inoue, M.; Fujikawa, R.; Baryshev, A.; Khanikaev, A.; Lim, P.; Uchida, H.; Aktsipetrov, O.; Fedyanin, A.; Murzina, T.; Granovsky, A. Magnetophotonic crystals. *J. Phys. Appl. Phys.* **2006**, *39*, R151. [CrossRef]

20.　Kahl, S.; Grishin, A.M. Enhanced Faraday rotation in all-garnet magneto-optical photonic crystal. *Appl. Phys. Lett.* **2004**, *84*, 1438–1440. [CrossRef]

21.　Dermeche, N.; Bouras, M.; Abdi-Ghaleh, R.; Kahlouche, A.; Hocini, A. Existence of high Faraday rotation and transmittance in magneto photonic crystals made by silica matrix doped with magnetic nanoparticles. *Optik* **2019**, *198*, 163225. [CrossRef]

22.　Lyubchanskii, I.; Dadoenkova, N.; Lyubchanskii, M.; Shapovalov, E.; Zabolotin, A.; Lee, Y.; Rasing, T. Response of two-defect magnetic photonic crystals to oblique incidence of light: Effect of defect layer variation. *J. Appl. Phys.* **2006**, *100*, 096110. [CrossRef]

23.　Pankin, P.S.; Vetrov, S.Y.; Timofeev, I.V. Tunable hybrid Tamm-microcavity states. *JOSA B* **2017**, *34*, 2633–2639. [CrossRef]

24.　Goto, T.; Dorofeenko, A.; Merzlikin, A.; Baryshev, A.; Vinogradov, A.; Inoue, M.; Lisyansky, A.; Granovsky, A. Optical Tamm states in one-dimensional magnetophotonic structures. *Phys. Rev. Lett.* **2008**, *101*, 113902. [CrossRef] [PubMed]

25.　Goto, T.; Baryshev, A.; Inoue, M.; Dorofeenko, A.; Merzlikin, A.; Vinogradov, A.; Lisyansky, A.; Granovsky, A. Tailoring surfaces of one-dimensional magnetophotonic crystals: Optical Tamm state and Faraday rotation. *Phys. Rev. B* **2009**, *79*, 125103. [CrossRef]

26.　Khanikaev, A.B.; Baryshev, A.V.; Inoue, M.; Kivshar, Y.S. One-way electromagnetic Tamm states in magnetophotonic structures. *Appl. Phys. Lett.* **2009**, *95*, 011101. [CrossRef]

27.　Levine, D.; Steinhardt, P.J. Quasicrystals: A new class of ordered structures. *Phys. Rev. Lett.* **1984**, *53*, 2477. [CrossRef]

28.　Shechtman, D.; Blech, I.; Gratias, D.; Cahn, J.W. Metallic phase with long-range orientational order and no translational symmetry. *Phys. Rev. Lett.* **1984**, *53*, 1951. [CrossRef]

29.　Vardeny, Z.V.; Nahata, A.; Agrawal, A. Optics of photonic quasicrystals. *Nat. Photonics* **2013**, *7*, 177–187. [CrossRef]

30.　Fu, X.; Liu, Y.; Zhou, P.; Sritrakool, W. Perfect self-similarity of energy spectra and gap-labeling properties in one-dimensional Fibonacci-class quasilattices. *Phys. Rev. B* **1997**, *55*, 2882. [CrossRef]

31.　Beck, M.; Geoghegan, R. *The Art of Proof: Basic Training for Deeper Mathematics*; Springer: Berlin/Heidelberg, Germany, 2010.

32.　Xu, P.; Tian, H.; Ji, Y. One-dimensional fractal photonic crystal and its characteristics. *JOSA B* **2010**, *27*, 640–647. [CrossRef]

33.　Segovia-Chaves, F.; Vinck-Posada, H. Transmittance spectrum in a 1D photonic crystal with a Fibonacci sequence composed of polymer materials. *Optik* **2019**, *196*, 163141. [CrossRef]

34.　Gong, Y.; Liu, X.; Wang, L.; Lu, H.; Wang, G. Multiple responses of TPP-assisted near-perfect absorption in metal/Fibonacci quasiperiodic photonic crystal. *Opt. Express* **2011**, *19*, 9759–9769. [CrossRef]

35. Lin, Z.; Kubo, H.; Goda, M. Self-similarity and scaling of wave function for binary quasiperiodic chains associated with quadratic irrationals. *Z. Für Phys. B Condens. Matter* **1995**, *98*, 111–118. [CrossRef]

36. Liu, N.h. Propagation of light waves in Thue-Morse dielectric multilayers. *Phys. Rev. B* **1997**, *55*, 3543. [CrossRef]

37. Liviotti, E. A study of the structure factor of Thue-Morse and period-doubling chains by wavelet analysis. *J. Phys. Condens. Matter* **1996**, *8*, 5007. [CrossRef]

38. Steurer, W.; Sutter-Widmer, D. Photonic and phononic quasicrystals. *J. Phys. D Appl. Phys.* **2007**, *40*, R229. [CrossRef]

39. Mehdizadeh, F.; Alipour-Banaei, H. Bandgap management in two-dimensional photonic crystal thue-morse structures. *J. Opt. Commun.* **2013**, *34*, 61–65. [CrossRef]

40. Moretti, L.; Mocella, V. Two-dimensional photonic aperiodic crystals based on Thue-Morse sequence. *Opt. Express* **2007**, *15*, 15314–15323. [CrossRef]

41. Loiko, V.; Miskevich, A. Optical properties of structures composed of periodic, quasi-periodic, and aperiodic sequences of particulate monolayers. *Opt. Spectrosc.* **2017**, *122*, 16–24. [CrossRef]

42. Xavier, J.; Probst, J.; Becker, C. Deterministic composite nanophotonic lattices in large area for broadband applications. *Sci. Rep.* **2016**, *6*, 1–12. [CrossRef]

43. Kasture, S.; Ravishankar, A.P.; Yallapragada, V.; Patil, R.; Valappil, N.V.; Mulay, G.; Achanta, V.G. Plasmonic quasicrystals with broadband transmission enhancement. *Sci. Rep.* **2014**, *4*, 1–6. [CrossRef]

44. Ghorbani-Oranj, F.; Abdi-Ghaleh, R.; Roumi, B.; Jamshidi-Ghaleh, K.; Madani, A.; Zhou, Y. Comparative study of Faraday rotation spectra of periodic and Fibonacci multilayer structures containing graphene sheets. *Phys. B Condens. Matter* **2022**, *636*, 413835. [CrossRef]

45. da Silva, R.; Zanetti, F.; Lyra, M.; de Oliveira, I. Polarization rotation of localized modes in magneto-photonic Fibonacci structures containing nematic layers. *Mol. Cryst. Liq. Cryst.* **2017**, *657*, 11–20. [CrossRef]

46. Zamani, M.; Amanollahi, M.; Taraz, M. Octonacci magnetophotonic quasi-crystals. *Opt. Mater.* **2019**, *88*, 187–194. [CrossRef]

47. Guo, S.J.; Hu, C.X.; Zhang, H.F. A reconfigurable device based on the one-dimensional magnetized plasma photonic crystals nested with the Pell and Thue–Morse sequences. *Opt. Quantum Electron.* **2020**, *52*, 1–18. [CrossRef]

48. Kalish, A.N.; Komarov, R.S.; Kozhaev, M.A.; Achanta, V.G.; Dagesyan, S.A.; Shaposhnikov, A.N.; Prokopov, A.R.; Berzhansky, V.N.; Zvezdin, A.K.; Belotelov, V.I. Magnetoplasmonic quasicrystals: An approach for multiband magneto-optical response. *Optica* **2018**, *5*, 617–623. [CrossRef]

49. Dotsenko, A.A.; Kalish, A.N.; Kozhaev, M.A.; Ignatyeva, D.O.; Achanta, V.G.; Zvezdin, A.K.; Belotelov, V.I. Magneto-optical effects in 2D plasmonic gratings with various types of ordering. *AIP Conf. Proc.* **2020**, *2300*, 020026.

50. Wu, J.; Wang, Z.; Wu, B.; Shi, Z.; Wu, X. The giant enhancement of nonreciprocal radiation in Thue-morse aperiodic structures. *Opt. Laser Technol.* **2022**, *152*, 108138. [CrossRef]

51. Guo, S.; Hu, C.; Zhang, H. Ultra-wide unidirectional infrared absorber based on 1D gyromagnetic photonic crystals concatenated with general Fibonacci quasi-periodic structure in transverse magnetization. *J. Opt.* **2020**, *22*, 105101. [CrossRef]

52. Guo, S.; Mao, M.; Zhou, Z.; Zhang, D.; Zhang, H. The wide-angle broadband absorption and polarization separation in the one-dimensional magnetized ferrite photonic crystals arranged by the Dodecanacci sequence under the transverse magnetization configuration. *J. Phys. D Appl. Phys.* **2020**, *54*, 015004. [CrossRef]

53. Wang, H.; Yu, B.; Cai, D.; Chen, K. Magneto-Optical Goos- Hänchen Displacement in Quasiperiodic Gradient 1D Photonic Crystal. *Phys. Status Solidi* **2022**, *259*, 2100624. [CrossRef]

54. Moharam, M.; Grann, E.B.; Pommet, D.A.; Gaylord, T. Formulation for stable and efficient implementation of the rigorous coupled-wave analysis of binary gratings. *JOSA A* **1995**, *12*, 1068–1076. [CrossRef]

55. Li, L. Fourier modal method for crossed anisotropic gratings with arbitrary permittivity and permeability tensors. *J. Opt. A Pure Appl. Opt.* **2003**, *5*, 345. [CrossRef]

56. Zvezdin, A.K.; Kotov, V.A. *Modern Magnetooptics and Magnetooptical Materials*; CRC Press: Boca Raton, FL, USA, 1997.

57. Ignatyeva, D.; Kapralov, P.; Knyazev, G.; Sekatskii, S.; Dietler, G.; Vasiliev, M.; Alameh, K.; Belotelov, V. High-Q surface modes in photonic crystal/iron garnet film heterostructures for sensor applications. *JETP Lett.* **2016**, *104*, 679–684. [CrossRef]

58. Ignatyeva, D.O.; Karki, D.; Voronov, A.A.; Kozhaev, M.A.; Krichevsky, D.M.; Chernov, A.I.; Levy, M.; Belotelov, V.I. All-dielectric magnetic metasurface for advanced light control in dual polarizations combined with high-Q resonances. *Nat. Commun.* **2020**, *11*, 1–8. [CrossRef]

59. Voronov, A.A.; Karki, D.; Ignatyeva, D.O.; Kozhaev, M.A.; Levy, M.; Belotelov, V.I. Magneto-optics of subwavelength all-dielectric gratings. *Opt. Express* **2020**, *28*, 17988–17996. [CrossRef] [PubMed]

60. Levy, M.; Borovkova, O.V.; Sheidler, C.; Blasiola, B.; Karki, D.; Jomard, F.; Kozhaev, M.A.; Popova, E.; Keller, N.; Belotelov, V.I. Faraday rotation in iron garnet films beyond elemental substitutions. *Optica* **2019**, *6*, 642–646. [CrossRef]

61. Belotelov, V.I.; Kalish, A.N.; Zvezdin, A.K.; Gopal, A.V.; Vengurlekar, A.S. Fabry–Perot plasmonic structures for nanophotonics. *JOSA B* **2012**, *29*, 294–299. [CrossRef]

62. Poddubny, A.; Pilozzi, L.; Voronov, M.; Ivchenko, E. Exciton-polaritonic quasicrystalline and aperiodic structures. *Phys. Rev. B* **2009**, *80*, 115314. [CrossRef]

63. Poddubny, A.; Ivchenko, E. Photonic quasicrystalline and aperiodic structures. *Phys. E Low-Dimens. Syst. Nanostruct.* **2010**, *42*, 1871–1895. [CrossRef]